IEEE Access
Multidisciplinary | Rapid Review | Open Access Journal

Received April 24, 2021, accepted May 2, 2021, date of publication May 6, 2021, date of current version June 2, 2021.

Digital Object Identifier 10.1109/ACCESS.2021.3078066

Dual Adaptive Nonlinear Droop Control of VSC-MTDC System for Improved Transient Stability and Provision of Primary Frequency Support

HAMED SHADABI, (Student Member, IEEE), AND INNOCENT KAMWA, (Fellow, IEEE)
Pavillon Adrien-Pouliot, Université Laval, Quebec City, QC G1V 0A6, Canada

Corresponding author: Hamed Shadabi (hamed.shadabi.1@ulaval.ca)

ABSTRACT This paper presents an adaptive nonlinear droop control (ANLDC) strategy for the voltage source converter (VSC) in multi-terminal high voltage direct current (MTDC) system, which enables the converters to provide primary frequency control for connected AC grids. The presented strategy inherits the concept of an emergency control approach. In normal condition when there is no significant deviation in RoCoF and DC voltage, it will be in inactive mode. The combination of two control techniques, nonlinear frequency-droop control, and nonlinear voltage-droop control results in a dual nonlinear controller that includes the advantages of both of them at the same time. The ANLDC strategy bears the advantage of the traditional droop control that is based on local measurements and there is no need for a communication system. The simulation results indicate that the AC/DC station with the proposed dual control strategy can improve simultaneously the primary frequency response and transient stability of the connected AC grid.

INDEX TERMS Droop control, frequency regulation, multi-terminal DC (MTDC) systems, primary frequency control (PFC), renewable energy, VSC-HVDC (high voltage direct current).

I. INTRODUCTION

The growing penetration of renewable energy sources especially offshore wind plants into the power system leads to challenges concerning grid stability, power quality, and inertia. The suitable technology for connecting offshore wind plants to the onshore AC power system is the VSC-HVDC transmission system. Currently, due to the development of VSC converter technology, the MTDC systems have emerged as economical alternative solutions for harvesting offshore wind energy [1]. VSC-HVDC system accelerated development resulted in building offshore wind farms (WFs) in far locations from onshore which are the potential sources of energy with cheap land [2]. The growing integration of renewable energy sources via power electronic converters in the United States during the last years has led to a decrease in system inertia on the eastern interconnection [3]. Definitely, the inertia reduction increases the probability of instability in the power system and thus requires mitigation means to support the system frequency [4]. Generally, the HVDC system attempts by several means to provide frequency support to the AC system through the connected offshore or onshore grids. A large number of investigations have been reported on this matter. Reference [5] proposed a method for providing frequency support between several AC areas via an MTDC system. In the suggested controller a universal N_{th}-order model was used to improve the droop gain in AC-side disturbance situations. The proposed strategy in [6] provides frequency support for an AC grid by wind turbines through an MTDC grid. The presented method can decrease the RoCoF and ameliorate the frequency response of the system. A novel decentralized control strategy based on inertial droop was proposed in [7] to provide desired frequency regulation during AC side events. Furthermore, utilizing the offshore wind farm potential to regulate the frequency of the connected AC grid through MTDC has been investigated. Reference [8] proposed a new generic frequency regulation method based on a global measured reference signal for the VSC converter to improve the interchange of primary reserves among AC grids connected via the MTDC system.

The associate editor coordinating the review of this manuscript and approving it for publication was Sanjeevikumar Padmanaban.

On the other hand, the presented technique reduces the interaction between the control loops of DC voltage and frequency. Hence, a frequency droop control strategy is presented in [9], [10] which tries to use the stored active power from the onshore converter to support frequency response. Analyzing the effects of droop gain correction on the frequency stabilization via local measurements is presented in [11]. Further, to improve the active power oscillations, a modified method that includes a low pass filter (LPF) and small dead-bands is suggested in that paper. Employing HVDC capacitors energy and wind turbines inertia simultaneously to provide inertia support for connected AC grid through local measurements is proposed in [2]. A new control scheme based on DC voltage manipulation is proposed for an MTDC grid in [12]. This control method attempts to minimize the frequency deviation by readjusting the active power of each terminal. An effective communication less four-terminal MTDC grid is introduced in [13] based on the identification and development of novel local VSC-HVDC controllers. VSC Inertia emulation strategy in an MTDC grid is investigated in [1]. To increase the operational flexibility, the presented strategy is implemented in the primary layer of the MTDC hierarchical control scheme. A unified reference controller (URC) is presented in [14] which enables a hybrid AC-DC system to eliminate the disturbance through sharing the inertia of strong AC grids with high inertia. Indeed, this emerged as an alternative solution for controlling the hybrid AC–DC system through the hierarchical power flow control mechanism of the MTDC grid [15]. A combination of frequency droop control and DC voltage droop control is given in [16] which enables AC grids connected via an MTDC network to provide frequency regulation support at the point of common coupling (PCC). The suggested method reacts to both AC and DC side power balance deviation. A new distributed frequency control through an MTDC grid is introduced in [17] to provide frequency and DC voltage regulation as well as reserves recovery of asynchronous areas. Interestingly, as a part of the hierarchical control scheme, this controller was designed based on local measurements. The operation of VSC to emulate the synchronous generator behavior is presented in [18]. This controller contains two layers: an internal layer for rapid control of current and voltage and an external layer for inertia mimicry. The VSCs control plays an important role to improve the AC system performance under transient situations such as during fault periods [19]. Several strategies have been proposed for fault ride through in VSC-HVDC transmission systems such as: decreasing the generated power by the wind turbines and a short circuit mimicry on the offshore station to decouple the onshore grid [19], [20]. On another hand, an MTDC grid can be complemented with a BESS to enable an adaptive fast frequency regulation strategy based on the modulation of the converter's power [21]. However, since the power reference variation resulting from the frequency droop controller leads to a DC voltage deviation, the proposed controller in [22] increases the probability of the DC system instability. To address this pitfall, several publications used the two droop controls simultaneously for a VSC based station. The main subject matter of [22] is the analysis of the eigenvalues of the MTDC system while [23] introduces the advantages of using a dead-band control for improving both frequency and voltage droop controls. Investigating the interactions between DC and AC networks by using modal analysis is given in [24]. Simultaneous use of frequency and voltage droops leads to improving the DC voltage deviation and frequency dips under transient situations. The previous survey convinced us that although progress has been made towards using VSC-MTDC grids to assist AC grid frequency response and transient stability separately, room for improvement remains when attempting to meet both goals simultaneously, in a satisfactory manner. Hence, this paper presents an adaptive nonlinear droop control method that enables the VSC converters of the MTDC grid to provide primary frequency support for the AC side especially for preventing temporary frequency deviation considering DC voltage stability and therefore improving transient stability of the AC grid. It is demonstrated how a simple nonlinear gain-based droop controller can be used for PFC over an MTDC grid. The proposed ANLDC strategy includes two control techniques. The first one is a frequency-based nonlinear droop control which provides frequency regulation for the connected AC grids and the second control strategy is the voltage droop nonlinear control method, which ensures a reliable and strong DC system. The main contributions highlighted in this research are summarized as follows:

1) A non-linear adaptive control-based technique is utilized to enable fast frequency regulation and DC grid voltage regulation across a wide range of local parameters.
2) Simultaneously, DC grid voltage regulation for transient stability enhancement of the AC-DC grid is achieved.

The remainder of this paper is organized as follows: Section II derives a mathematical model of the studied system, while Section III provides frequency support requirements for frequency control in MTDC systems. In Section IV, the simulation results are discussed, and the conclusions are presented in Section V.

II. SYSTEM MODELING

A. MTDC-CONNECTED AC GRID

This study focuses on an MTDC system connected to the AC grid as shown in Fig. 1. At the elementary level, a simplified model of the MTDC can be considered assuming its connection to the main AC grid consisting of a multi-machine main power system. By considering a common frequency f for all generators and slight deviations of the frequency around its nominal value, the well-known swing equation of the system for a sudden disconnection of the generator k, can

be considered as follows:

$$\frac{d}{dt}\Delta f(t) = \frac{f_0}{2H}(\Delta P_m(t) + \Delta P_{VSC}(t) - P_{ek} + P_{L_{sh}} - D\Delta f(t)) \quad (1)$$

With H: Equivalent inertia constant, calculated by

$$H = \frac{1}{S_{base}} \sum_{i=1, i\neq j}^{n} H_i S_{bi} \quad (2)$$

f_0: Rated frequency.
$\Delta P_m(t)$: Increment of the mechanical power via primary controllers

$$\frac{d}{dt}\Delta P_m(t) + \frac{\Delta P_m(t)}{T_g} = -\frac{\Delta f(t)}{R_p T_g} \quad (3)$$

R_p: Equivalent droop constant.
T_g: Equivalent governor-turbine time constant.
$\Delta P_{VSC}(t)$: Increment of the Injected power by VSC.
P_{ek}: The pre-disturbance output power of generator k.
$P_{L_{sh}}$: Load shed (considered 0.1 pu).
D: Damping due to frequency sensitivity of loads.

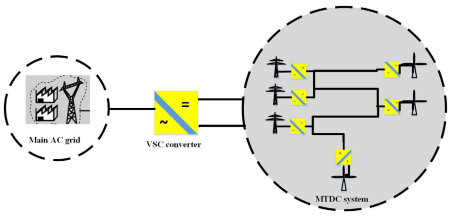

FIGURE 1. An MTDC-connected main AC grid.

As it appeared from equation (1), the frequency response of the system depends on different parameters such as inertia constant H, primary mechanical injected power, VSC rating, and the capacity of disconnected generator and load. To illustrate the influence of each parameter on the system frequency response, the system swing equation is modeled and simulated as shown in Fig. 2.

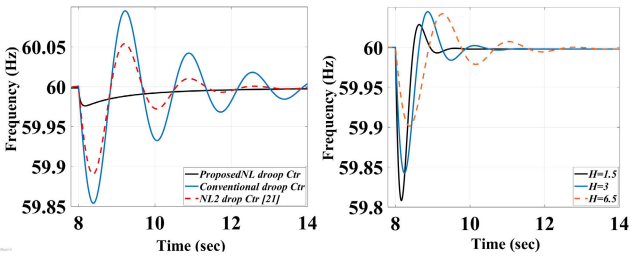

FIGURE 2. Frequency response trajectories for varying system parameters and different droop control strategies.

For frequency regulation of the onshore grid, the frequency-DC voltage controller is proposed for Grid Side-VSC to achieve the desired results considering the limitation of the frequency droop in AC grid and DC voltage droop in the DC link. The general representation of the suggested control strategy is illustrated in Fig. 3.

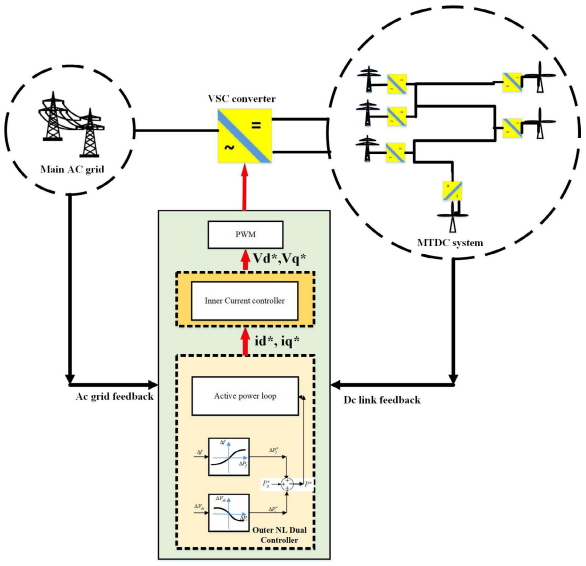

FIGURE 3. Whole structure of the proposed ANLDC.

B. DYNAMIC MODELING OF THE MTDC SYSTEM

To perform transient or steady-state analysis of the MTDC studied system, its dynamic model is derived in this section. A simple representation is considered for the AC-DC connection system as illustrated in Fig. 4. By neglecting the converter switching dynamic, the state-space model of the MTDC system can be obtained as follows:

$$\frac{d}{dt}V_{DC_i} = \frac{1}{C_i}(I_{DC_i} - \sum I_{ij}) \quad (4)$$

$$\frac{d}{dt}I_{ij} = -\frac{1}{L_{ij}}(R_{ij}I_{ij} + V_{DC_i} - V_{DC_j}), \quad \forall i \in N_{line} \quad (5)$$

$$C_i = C_{DC_i} + \frac{\sum C_{ij}}{2} \quad (6)$$

where $N_{B_{DC}}$ is the number of DC bus and N_{line} is the number of DC line. By considering the line currents and DC bus voltages as states, the state-space model of an MTDC system is given as follows:

$$\dot{X} = AX + BU$$
$$Y = CX + DU \quad (7)$$

where

$$X = [I_1 \dots I_{line}\ V_1 \dots V_{N_{B_{DC}}}\ f_i\ P_{mi}]$$
$$U = [V_1^{rated} \dots V_{N_{droop}}^{rated}\ I_{DC_{N_{droop}+1}} \dots\dots I_{N_{B_{DC}}}\ f_i\ P_{mi}\ P_{outage}] \quad (8)$$

With N_{droop} the number of converters equipped with droop controller while f_i, P_{outage}, and P_{mi} are respectively the frequency, power outage in AC side and the prime mover power of the i^{th} converter equipped with the NL droop controllers.

III. FREQUENCY SUPPORT REQUIREMENTS

To provide fast frequency regulation, the injected power to the AC grid must be modulated. This purpose can in turn be

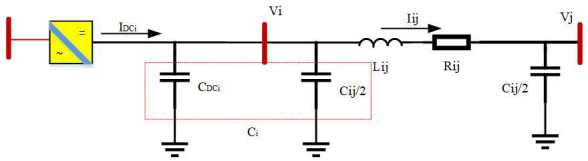

FIGURE 4. An AC-DC connection system.

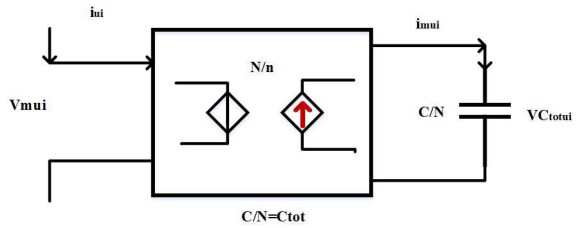

FIGURE 5. Equivalent circuit of an MMC arm [25].

fulfilled from two different embedded sources of energy: one is energy stored in the MTDC and the other is a dedicated energy storage system such as a BESS.

A. MTDC RESPONSE

The first type of VSC is the two-level converter. In such a system the AC output signal is provided by switching between the positive and negative polarities of the DC side. An effective option to improve the quality of the AC output waveform is using pulse width modulation (PWM) technique. During the last years, the modular multilevel converter has represented unique progress compared with the conventional two-level converters. It presents some new advantages such as modularity, efficiency, harmonic Performance [25]. By neglecting the series inductance and resistance of the DC cable due to the fast dynamic of the DC network, all the DC capacitances can be represented by an equivalent capacitance C_{totdc}. Therefore the stored energy in the Dc side of the MTDC grid can be calculated as:

$$E_{C_{MTDC}} = \frac{1}{2}C_{totdc}V_{DC}^2(t),\ P(t) = C_{totdc}V_{DC}(t)\frac{d}{dt}V_{DC}(t) \quad (9)$$

An imbalance between the total injected power (P_{rec}) and extracted power (P_{inv}) of the DC grid will lead to deviation of DC voltage from its desired value through charge or discharge capacity C_{totdc}.

$$V\frac{dV}{dt} = \frac{P_{rec} - P_{inv}}{2H_{dc}^{tot}} \quad (10)$$

H_{dc}^{tot} is defined as the electrostatic constant of the MTDC. It can be considered as the equivalent of the inertia constant in the swing Equation of an AC system [26].

$$H_{dc}^{tot} = \frac{1}{2}C_{totdc}^{pu}\frac{V_b^2}{P_b} \quad (11)$$

Due to the MMC technology's high energy storage capability, it becomes more feasible to use the stored energy in the VSC converters [27]. The equivalent model of the MMC contains total capacitors, inductors, and resistances. By considering the model of Fig. 5 as the equivalent circuit of an MMC arm, the total equivalent capacitors can be considered as the main energy storage system in the MMC. The stored energy in an arm of MMC (in the upper arm) can be derived as:

$$W_{ctot.ui} = \frac{1}{2}C_{tot}V_{ctot.ui}^2 \quad (12)$$

$V_{C_{tot_{ui}}}$: the sum of all capacitor voltages within i_{th} upper arm.

C_{tot}: equivalent capacitance of each arm.

$V_{m_{ui}}$: sum of the sub-modules voltages within an upper arm.

i_{ui}: current of an upper arm.

i_m: the current of equivalent capacitance of each arm.

N: number of series-connected submodules.

B. PROPOSED ANLDC

The main benefit of VSC converter frequency response is its fast response that enables the system to support the AC grid through a fast inertial response. However, the stored energy that is normally available in the DC link of an MTDC system is limited and to achieve a low boundary of the thermal plants inertia, large capacitance is required.

Two strategies can be considered for providing frequency regulation via MTDC grids: (i) continual acting support, and (ii) emergency acting support. In the second control strategy, the frequency support is activated by detecting an unusual change of RoCoF [26]. Hence, a modified fast frequency regulation method based on PLL frequency measurement is introduced in [21]. The converter droop reference based on the proposed droop control strategy is calculated as follows [21]:

$$\Delta P_{ref} = K_A|\Delta f|\Delta f \quad (13)$$

The stored energy in an MTDC system's DC link is restricted, and while the output of the variable droop gain proposed in [19] is dependent on the frequency deviation of the system, it contributes to small deviations in the power reference of the VSC, as shown in Fig. 7, which can result in poor controller efficiency under significant frequency deviations. A single frequency droop controller attempts to regulate the frequency by making use of the stored energy in the DC link which results in the DC voltage deviation. To improve this deficiency and provide frequency support to the interconnected AC grids while having a reliable DC grid, a dual nonlinear controller is presented here which is a combination of two control techniques. The proposed controller in this study bears the spirit of an emergency concept, since in normal conditions when there is no significant big deviation in RoCoF and DC voltage, it will remain in the inactive mode. The strategy proposes an integral control with an adaptive gain. The block diagram of the proposed ANLDC

strategy is shown in Fig. 6. The rationale behind this idea is that the permissible frequency deviation for a grid is about 1% of the rated frequency in normal continuous operation. Due to the small scale of frequency (and voltage) changes, the amount of the injected power by the conventional droop control is not considerable. To address this shortcoming and improve the effectiveness of the droop controller and avoid a frequent response to small random deviations, a suitable dual nonlinear droop control scheme is adopted here. For the proposed structure in Fig. 6, by considering VSC_i as a converter controlled by the dual nonlinear controller with the square root function, the power reference deviation of the converter can be calculated as follows:

$$\Delta P_{VSCi} = \Delta P_{fi} + \Delta P_{vi} \tag{14}$$

$$\begin{cases} \Delta P_{fi} = (K_{AF}\sqrt{|f_{refi} - f_i|}).(f_{refi} - f_i) = K_{DF.NL}\Delta f_i \\ \Delta P_{vi} = (K_{Av}\sqrt{|V_{DCref} - V_{DC}|}).(V_{DCref} - V_{DC}) \\ = K_{DV.NL}\Delta V_{DC} \end{cases} \tag{15}$$

where:

$$K_{DF.NL} = (K_{AF}\sqrt{|f_{refi} - f_i|}) \tag{16}$$

$$K_{DV.NL} = (K_{Av}\sqrt{|V_{DCref} - V_{DC}|}) \tag{17}$$

Equations (16) and (17) reveal that the droop gains are proportional to the roots of the measured absolute value of DC voltage and frequency deviance from the rated value. By using the nonlinear characteristic for the droop controller, the injected power of converter changes non-linearly with the frequency (and voltage) amplitude changes. As a result, the converter power deviation (14) is nonlinearly proportional to the DC voltage and frequency deviations. Because the RoCoF remains in a small range of variations, the proposed droop control results in nonlinear droop curves for frequency and DC voltage regulations. According to Fig. 7, the reaction of the controller to the voltage and frequency variations is increased nonlinearly by increasing the deviations. When the frequency deviance from the rated value is inside the accepted bound (around the rated value), the power deviation of the converter will be smaller compared to the traditional linear droop. When the part of the controller (the part related to frequency deviation) tries to compensate the power deficiency by using the stored energy in the DC grid, the other part of the controller (the part related to DC voltage deviation) attempts to prevent the violation of the DC voltage deviation limitation.

The proposed control framework allows the VSC to regulate the frequency of an AC grid-connected MTDC while taking into account the DC voltage drop limit. ANLDCs are triggered when a disruption occurs and provide a power reference signal based on equations (14) and (15). Furthermore, as seen in fig 7, good dynamic performance as an emergency acting support under both nonlinear droop curves was obtained by local measurements. However, the simultaneous use of the two droops results in a kind of interaction between Voltage and frequency controllers. Existing coupling between the two nonlinear droop controls used in the proposed strategy

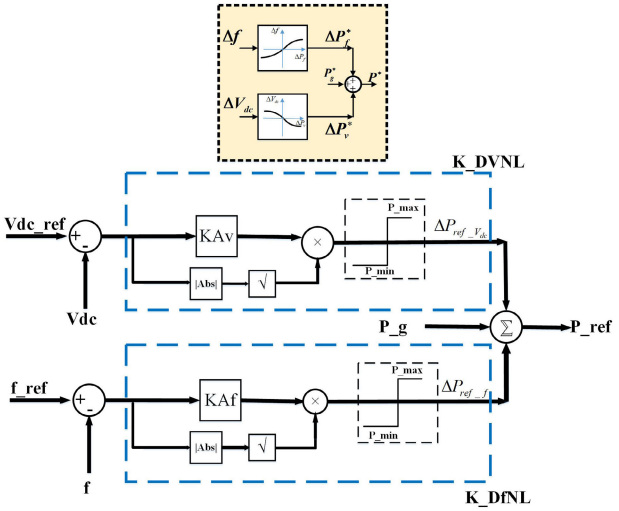

FIGURE 6. The block diagram of proposed ANLDC.

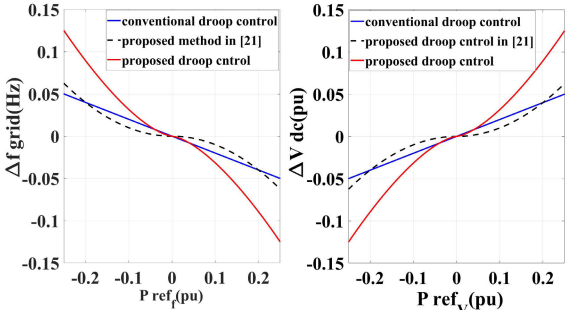

FIGURE 7. Resultant Droop Curve of ANLDC.

gives rise to the DC voltage stability besides the frequency regulation of the interconnected AC grid.

C. INTERACTIONS BETWEEN VOLTAGE AND FREQUENCY ANLDC

Using voltage and frequency droop controllers together brings about a kind of coupling between them. For example, if the AC grid frequency decreases, the frequency droop control modifies the injected power of the converter so that the DC voltage will decline. In this situation, the voltage droop controller opposes the DC voltage deviation. By neglecting the power losses in the DC grid, the DC voltage deviation can be described as:

$$\Delta V_{DC_i} = \Delta V_{DC}, \quad \forall i \in \{1, \ldots, m\} \tag{18}$$

After a disturbance at the AC side for instance load variations or a generator outage, the sum of the resulting converter power deviations in an MTDC system with m converters is described as follows:

$$\sum_{i=1}^{n} \Delta P_i = \sum_{i=1}^{n} K_{DfNL_i}\Delta f_i + \sum_{i=1}^{n} K_{DVNL_i}\Delta V_{DC} \tag{19}$$

Since the DC grid power is regulated by the stations controlled with a droop control, (19) can be written as:

$$\sum_{i=1}^{n} \Delta P_i = 0 \tag{20}$$

$$\Delta V_{DC} = -\frac{\sum_{i=1}^{n} K_{DfNL_i} \Delta f_i}{\sum_{i=1}^{n} K_{DVNL_i}} \tag{21}$$

For the j^{th} MTDC grid converter, replacing (21) in (19) results in:

$$\Delta P_j = K_{DfNL_i} \Delta f_i + K_{DVNL_i}(-\frac{\sum_{i=1}^{n} K_{DfNL_i} \Delta f_i}{\sum_{i=1}^{n} K_{DVNL_i}}) \tag{22}$$

Assuming that there is no disturbance in the AC side of the other AC grids simultaneously, their respective frequency deviations can be neglected. Therefore (22) can be rewritten as:

$$\Delta P_j = K_{DfNL_i} \Delta f_i (1 - \frac{K_{DfNL_j}}{\sum_{i=1}^{n} K_{DVNL_i}})) \tag{23}$$

According to (23) the power deviation of the j^{th} converter depends on:

- The sum of all voltage based nonlinear control droop gains
- The frequency based nonlinear control droop gain of the j^{th} converter

IV. SIMULATION AND RESULTS

DC3-CIGRE B4 DC benchmark grid, shown in Fig. 8 is used to evaluate the proposed control strategy. All the lines in this figure represent three lines for AC and two lines for DC grids. The CIGRE B4 working team has proposed the CIGRE DC test grid as a benchmark system for analyzing and evaluating DC grids studies [28], [29]. This test system consists of 11 AC-DC converters, 2 DC-DC converters, and 3 DC systems, namely DCS1, DCS2, and DCS3 [28]. The main parameters of the DC grid and stations are listed in TABLEs 1 and 2, respectively. To examine the efficiency of the proposed strategy, two simulation models are presented in this section.

- The equivalent Point to Point model consists of two simulated models for a simple two-terminal HVDC system. In the first simulation, an equivalent model is used to simulate the main AC grid and in the second simulation, the main AC grid is replaced with the two-area four machines grid.
- AC Grid Generation Shortage model includes the DC3-CIGRE B4 benchmark model and the AC grid.

TABLE 1. Line data [27].

Line Data	R [$\frac{\Omega}{Km}$]	L [$\frac{mH}{Km}$]	C [$\frac{\mu F}{KM}$]	G [$\frac{\mu S}{KM}$]
DC OHL	0.0114	0.9356	0.0123	-
DC cable	0.011	2.615	0.1908	0.048
AC OHL	0.0200	0.8532	0.0135	-

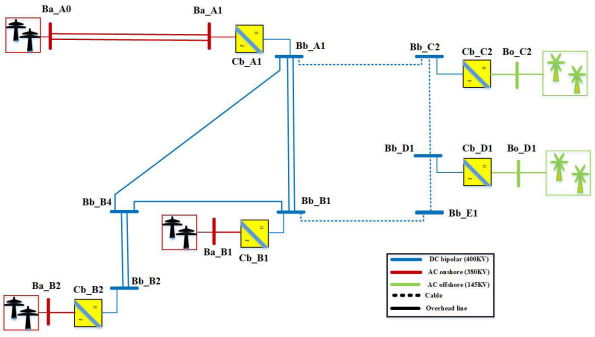

FIGURE 8. DCS3 single line diagram (part of Cigre B4 dc test grid).

TABLE 2. Converters parameters [27].

VSC Station	R [Ω]	L [mH]	C [μF]
$C_b - A_1$	0.403	33	450
$C_b - B_1$	0.403	33	450
$C_b - B_2$	1.21	98	150
$C_b - D_1$	0.65	49	300

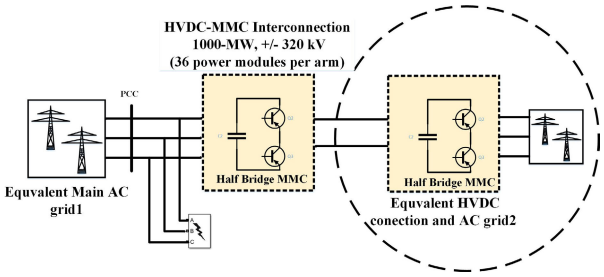

FIGURE 9. Point to Point HVDC system.

A. EQUIVALENT POINT TO POINT MODEL

This simulation has been done to illustrate how the presented control method performs under a fault situation on the AC side. The two-terminal equivalent grid is presented in Fig. 9. For a three-phase fault duration 0.1 s which occurred at the point of common coupling (PCC) at $t = 9\ s$, the active power, the DC voltage, and DC current of the converter station, with and without proposed ANLDC are shown in Fig. 10 and Fig. 11, respectively. As it can be apperceived from the simulation results in Fig. 11, after clearing the fault in AC side, the ANLDC of the grid-side converter tries to recover the power equilibrium in the system. In sharp contrast, the system is unable to restore a good service quality after fault clearing without ANLDC, as it appears that the DC voltage is trending towards instability.

In fact, TABLE 3 demonstrates that the ANLDC use the converters short-term active power capability to extend the critical clearing time (CCT)of the design contingency by more than a factor of 3. CCT stands for the maximum amount of time that a disruption can be removed without affecting the system's operation. The fault length is gradually increased until the system's instability threshold is reached to obtain the CCT.

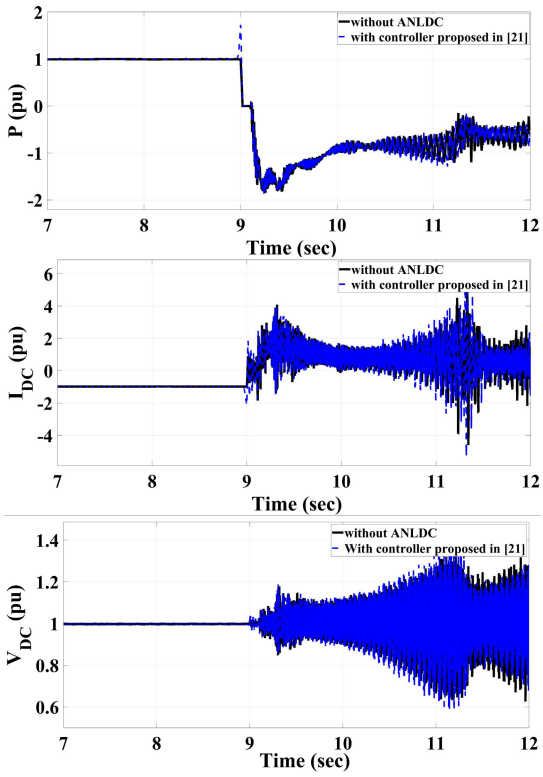

FIGURE 10. Active powers, voltage and DC current at the converter station.

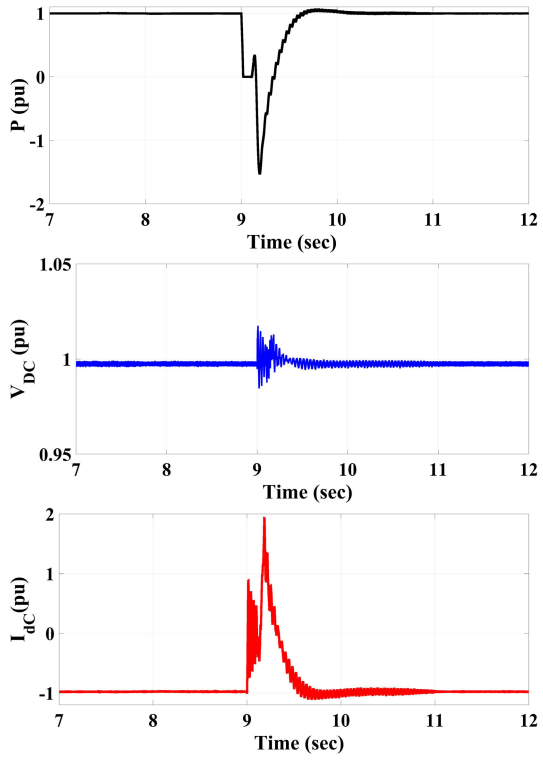

FIGURE 11. Active powers, voltage and DC current at the converter station with ANLDC.

To evaluate the performance of the suggested control strategy under even more realistic power grid conditions, the main

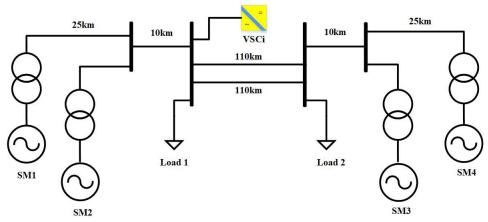

FIGURE 12. The two-area four-machines AC grid single-line diagram.

TABLE 3. CCT of fault.

Control mode	Without ANLDC	With ANLDC
Critical clearing time	37 ms	120 ms

TABLE 4. Generators data.

P_G(MVA)	V_N(KV)	H(s)	X_d (pu)	X_q (pu)
200	13.8	3.2	1.3	0.47

TABLE 5. Turbine governor and exciter data.

Turbine governor			
R_p	T_d(s)	T_a(s)	T_w(s)
0.05	0.01	0.07	2.67
Exciter			
T_r	T_a(s)	K_a(s)	K_e(s)
0.02	0.001	200	1

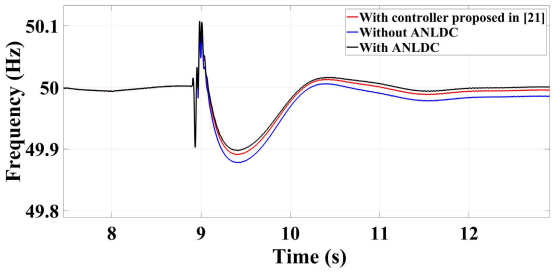

FIGURE 13. Frequency of the station VSC_i.

AC grid was replaced with the two-area four machines grid from [30] as shown in Fig. 12. The information of the AC grid are summarized in the TABLEs 4 and 5. At $t = 8.9\ s$ the generator SM4 is disconnected from the grid. The AC grid frequency and the output power of the VSC_i are illustrated in Fig. 13 and Fig. 14 respectively for this generator shedding event.

B. AC GRID GENERATION SHORTAGE

This part of the simulation addresses the performance of the presented controller with right the outage of generation in the AC grid connected to DC3-CIGRE B4. The four-machines AC grid, shown in Fig. 12, is connected to the MTDC via Ba–B2 station. During the simulation, the SM4 is disconnected from the grid at $t = 2\ s$ and results in power deficiency in the AC grid. Following this event, the injected power by the VSC of station Cb–B2 is increased because of its ability to provide frequency support. This leads to a DC voltage

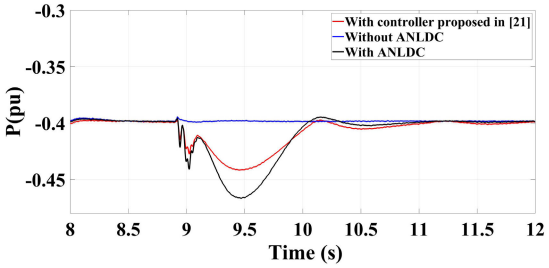

FIGURE 14. Active power of the station VSC_i.

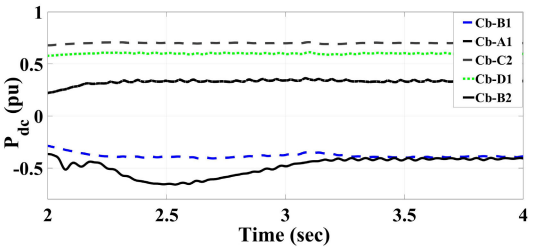

FIGURE 15. Active powers at converter stations.

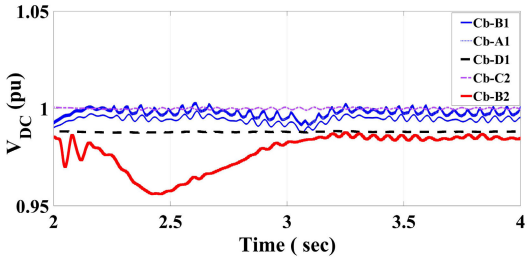

FIGURE 16. Stations DC voltage.

reduction. The voltage droop controller opposes the action of the frequency droop controller and prevents further DC voltage drop. The active power and DC voltage of all converter stations are shown in Fig. 15 and Fig. 16, respectively.

Furthermore, to demonstrate the desirable effects of the presented control strategy on the system operation, a comparison between two situations, with and without the proposed controller on the voltage and power of station Cb–B2 are shown in Figs. 17 and 18.

The frequency of the Ba–b2 within the simulation time is illustrated in Fig. 19. As is obvious from the results, the proposed control strategy is able to maintain the AC grid frequency at the nominal rate without impairing the DC voltage stability.

By applying three-phase fault at the point of common coupling (PCC) at $t = 3\ s$, the active power, and the DC voltage, of the converter station, and the frequency of the AC grid with and without proposed ANLDC are shown in Fig. 20, Fig. 21 and Fig. 22, respectively. After clearing the fault at $t = 3.1\ s$ on the AC side, the grid-side converter's ANLDC attempts to restore power equilibrium in the system, as seen in the simulation results. In comparison, without ANLDC,

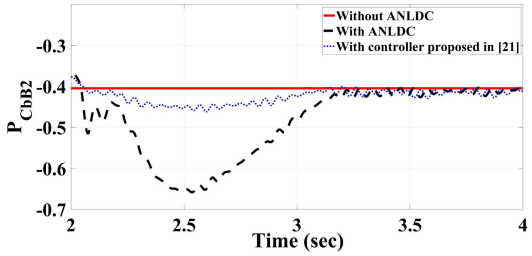

FIGURE 17. Power of station Cb–B2.

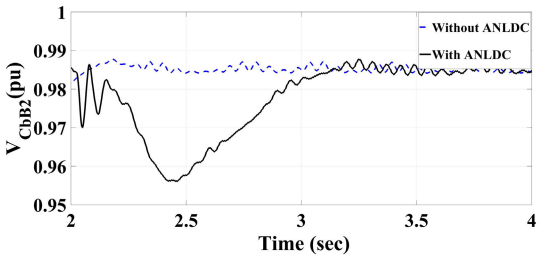

FIGURE 18. Voltage of station Cb–B2.

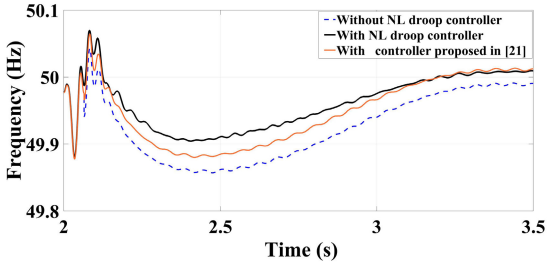

FIGURE 19. Frequency of the Ba–b2.

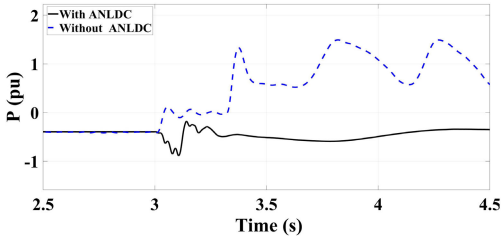

FIGURE 20. Active power of the Ba–b2.

the system is unable to recover good service efficiency after fault clearing, as the DC voltage tends to be trending towards instability. The CCT in the fault case can be obtained by gradually increasing the fault duration. TABLE 6 shows how the ANLDC makes use of the converter's short-term active power capacity to extend the fault's critical clearing time by around three times.

C. EFFECTS OF NON-LINEARLY CHANGING DROOP GAINS

Considering the modeling explained in section II-B, the state-space model of the DC3-CIGRE grid is derived from (8). As shown in Fig. 23, the small-signal stability study

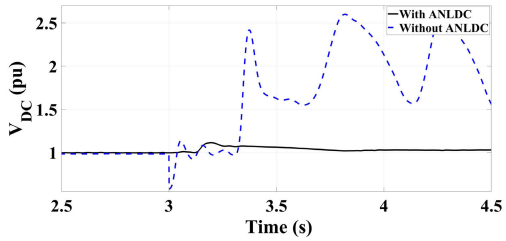

FIGURE 21. DC voltage of the Ba–b2.

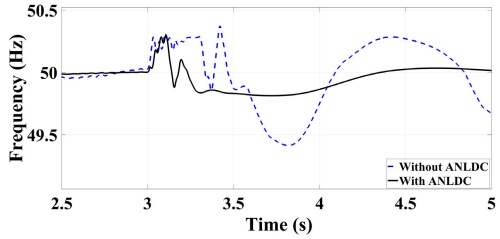

FIGURE 22. Frequency of the Ba–b2.

TABLE 6. CCT of fault.

Control mode	Without ANLDC	With ANLDC
Critical clearing time	56 ms	147 ms

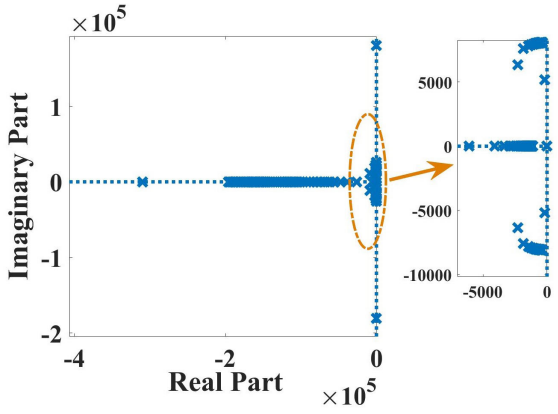

FIGURE 23. Movement of the eigenvalues due to the nonlinearly incremental of droop gain from 0 to 1.

indicates that the system will be stable for all non-linear gain values while it is apparent that the system eigenvalues become progressively negative as the droop gains increase nonlinearly, which gives rise to improving transient performance and stability.

V. CONCLUSION

This paper proposed an adaptive nonlinear dual controller applying frequency and voltage droops at the same time for efficient control of the VSC in MTDC grids. The proposed approach enables the VSC converters to provide short-term frequency support for the AC side and improve the DC grid stability. The presented dual ANLDC is a workable alternative to conventional droop strategies because it provides the benefits of the frequency and voltage droops simultaneously. The performance of the suggested strategy has not only been proven for the point-to-point HVDC system but also in the case of connecting an AC grid to the MTDC grid, it leads to satisfactory results. In this manner, the MTDC system assists regulating DC voltage and frequency in DC and AC grids respectively. Simulation results on the point to point HVDC system and DC3-CIGRE B4 DC benchmark grid have demonstrated the effective system performance through the presented nonlinear dual controller.

REFERENCES

[1] W. Zhang, K. Rouzbehi, A. Luna, G. B. Gharehpetian, and P. Rodriguez, "Multi-terminal HVDC grids with inertia mimicry capability," *IET Renew. Power Gener.*, vol. 10, no. 6, pp. 752–760, Jul. 2016.

[2] A. Junyent-Ferre, Y. Pipelzadeh, and T. C. Green, "Blending HVDC-link energy storage and offshore wind turbine inertia for fast frequency response," *IEEE Trans. Sustain. Energy*, vol. 6, no. 3, pp. 1059–1066, Jul. 2015.

[3] J. W. Ingleson and D. M. Ellis, "Tracking the eastern interconnection frequency governing characteristic," in *Proc. IEEE Power Eng. Soc. Gen. Meeting*, Jun. 2005, pp. 1461–1466.

[4] J. Zhu, C. D. Booth, G. P. Adam, A. J. Roscoe, and C. G. Bright, "Inertia emulation control strategy for VSC-HVDC transmission systems," *IEEE Trans. Power Syst.*, vol. 28, no. 2, pp. 1277–1287, May 2013.

[5] S. G. Vennelaganti and N. R. Chaudhuri, "Controlled primary frequency support for asynchronous AC areas through an MTDC grid," in *Proc. IEEE Power Energy Soc. Gen. Meeting (PESGM)*, Aug. 2018, pp. 1–5.

[6] M. Mehrabankhomartash, M. Saeedifard, and A. Yazdani, "Adjustable wind farm frequency support through multi-terminal HVDC grids," *IEEE Trans. Sustain. Energy*, vol. 12, no. 2, pp. 1461–1472, Apr. 2021.

[7] S. G. Vennelaganti and N. R. Chaudhuri, "Ratio-based selective inertial and primary frequency support through MTDC grids with offshore wind farms," *IEEE Trans. Power Syst.*, vol. 33, no. 6, pp. 7277–7287, Nov. 2018.

[8] Q. Zhang, J. D. McCalley, V. Ajjarapu, J. Renedo, M. A. Elizondo, A. Tbaileh, and N. Mohan, "Primary frequency support through North American continental HVDC interconnections with VSC-MTDC systems," *IEEE Trans. Power Syst.*, vol. 36, no. 1, pp. 806–817, Jan. 2021.

[9] T. M. Haileselassie, R. E. Torres-Olguin, T. K. Vrana, K. Uhlen, and T. Undeland, "Main grid frequency support strategy for VSC-HVDC connected wind farms with variable speed wind turbines," in *Proc. IEEE Trondheim PowerTech*, Jun. 2011, pp. 1–6.

[10] Y. Pipelzadeh, B. Chaudhuri, and T. C. Green, "Inertial response from remote offshore wind farms connected through VSC-HVDC links: A communication-less scheme," in *Proc. IEEE Power Energy Soc. Gen. Meeting*, Jul. 2012, pp. 1–6.

[11] L. Shen, M. Barnes, R. Preece, and J. Milanovic, "Frequency stabilisation using VSC-HVDC," in *Proc. IEEE Power Energy Soc. Gen. Meeting (PESGM)*, Jul. 2016, pp. 1–5.

[12] Y. Li, Z. Xu, J. Ostergaard, and D. J. Hill, "Coordinated control strategies for offshore wind farm integration via VSC-HVDC for system frequency support," *IEEE Trans. Energy Convers.*, vol. 32, no. 3, pp. 843–856, Sep. 2017.

[13] L. Xu, J. Rafferty, Y. Wang, and G. Xu, "MTDC systems for frequency support base on DC voltage manipulation," in *Proc. Int. Conf. Renew. Power Gener. (RPG)*, Oct. 2015, pp. 1–6.

[14] K. Rouzbehi, W. Zhang, J. I. Candela, A. Luna, and P. Rodriguez, "Unified reference controller for flexible primary control and inertia sharing in multi-terminal voltage source converter-HVDC grids," *IET Gener., Transmiss. Distrib.*, vol. 11, no. 3, pp. 750–758, Feb. 2017.

[15] R. Shah, J. C. Sanchez, R. Preece, and M. Barnes, "Stability and control of mixed AC–DC systems with VSC-HVDC: A review," *IET Gener., Transmiss. Distrib.*, vol. 12, no. 10, pp. 2207–2219, Jan. 2018.

[16] T. M. Haileselassie and K. Uhlen, "Primary frequency control of remote grids connected by multi-terminal HVDC," in *Proc. IEEE PES Gen. Meeting*, Jul. 2010, pp. 1–6.

[17] M. Andreasson, R. Wiget, D. V. Dimarogonas, K. H. Johansson, and G. Andersson, "Distributed frequency control through MTDC transmission systems," *IEEE Trans. Power Syst.*, vol. 32, no. 1, pp. 250–260, Jan. 2017.

[18] M. Guan, W. Pan, J. Zhang, Q. Hao, J. Cheng, and X. Zheng, "Synchronous generator emulation control strategy for voltage source converter (VSC) stations," *IEEE Trans. Power Syst.*, vol. 30, no. 6, pp. 3093–3101, Nov. 2015.
[19] W. Wang and M. Barnes, "Power flow algorithms for multi-terminal VSC-HVDC with droop control," *IEEE Trans. Power Syst.*, vol. 29, no. 4, pp. 1721–1730, Jul. 2014.
[20] T. D. Vrionis, X. I. Koutiva, N. A. Vovos, and G. B. Giannakopoulos, "Control of an HVDC link connecting a wind farm to the grid for fault ride-through enhancement," *IEEE Trans. Power Syst.*, vol. 22, no. 4, pp. 2039–2047, Nov. 2007.
[21] T. Zhang, J. A. Orr, and A. E. Emanuel, "Adaptable energy storage system control for microgrid stability enhancement," in *Proc. IEEE Power Energy Soc. Gen. Meeting (PESGM)*, Aug. 2018, pp. 1–5.
[22] T. K. Vrana, L. Zeni, and O. B. Fosso, "Active power control with undeadband voltage & frequency droop for HVDC converters in large meshed DC grids," in *Proc. EWEA Conf.*, Copenhagen, Denmark, Apr. 2012, pp. 1–8.
[23] N. R. Chaudhuri, R. Majumder, and B. Chaudhuri, "System frequency support through multi-terminal DC (MTDC) grids," *IEEE Trans. Power Syst.*, vol. 28, no. 1, pp. 347–356, Feb. 2013.
[24] P. Rault, X. Guillaud, F. Colas, and S. Nguefeu, "Investigation on interactions between AC and DC grids," in *Proc. IEEE Grenoble Conf.*, Jun. 2013, pp. 1–6.
[25] S. Samimi, "Modélisation et commande des convertisseurs mmc en vue de leur intégration dans le réseau électrique," Ph.D. dissertation, Dept. Elect. Eng., Ecole Centrale de Lille, Villeneuve-d'Ascq, France, 2018.
[26] L. Papangelis, "Local and centralized control of multi-terminal dc grids for secure operation of combined AC/DC systems," Ph.D. dissertation, Département d'Electricité, Electroniqueet Informatique, Université de Liége, Liége, Belgique, 2018.
[27] S. Rohner, S. Bernet, M. Hiller, and R. Sommer, "Modulation, losses, and semiconductor requirements of modular multilevel converters," *IEEE Trans. Ind. Electron.*, vol. 57, no. 8, pp. 2633–2642, Aug. 2010.
[28] *Comité d'études B4, Guide for the Development of Models for HVDC Converters in a HVDC Grid*, C. International Grands RéseauxÉlectriques, Paris, France, 2014.
[29] K. Rouzbehi, A. Miranian, A. Luna, and P. Rodriguez, "DC voltage control and power sharing in multiterminal DC grids based on optimal DC power flow and voltage-droop strategy," *IEEE J. Emerg. Sel. Topics Power Electron.*, vol. 2, no. 4, pp. 1171–1180, Dec. 2014.
[30] P. Kundur, N. J. Balu, and M. G. Lauby, *Power System Stability and Control*, vol. 7. New York, NY, USA: McGraw-Hill, 1994.

HAMED SHADABI (Student Member, IEEE) received the M.S. degree from the University of Tabriz, Iran, in 2014. He is currently pursuing the Ph.D. degree with the University of Laval, Québec City, Canada. Since April 2020, he has been an Intern at IREQ. His research interests include HVDC transmission systems, power grid transient reliability, clean energies, and ESSs use of power systems.

INNOCENT KAMWA (Fellow, IEEE) received the B.S. and Ph.D. degrees in electrical engineering from Laval University, Québec City, in 1985 and 1989, respectively. He had been a Research Scientist and a Registered Professional Engineer with the Hydro-Quebec Research Institute, since 1988, specializing in system dynamics, power grid control and renewable energy integration. After leading system automation and control program for years, he became the Chief Scientist for smart grid, in 2009, the Chief of power system and mathematics, in 2014, overseeing the Hydro-Quebec Network Simulation Centre known worldwide, and the Acting Scientific Director of IREQ, in 2016. Since 1990, he has been an Adjunct Professor in electrical engineering with Laval University and McGill University, since 2011. He has also been an Associate Editor of *International Journal on Electrical Power Energy Systems*, IEEE TRANSACTIONS ON POWER SYSTEMS, and IEEE POWER AND ENERGY SOCIETY (PES) LETTERS, and the Editor-in-Chief of *IET Generation, Transmission and Distribution*, since 2012.